PHILOSOPHICAL TRANSACTIONS OF THE ROYAL SOCIETY B BIOLOGICAL SCIENCES

A Method for Routine Monitoring of the Aerial Migration of Insects by Using a Vertical-Looking Radar

A. D. Smith, J. R. Riley and R. D. Gregory

Phil. Trans. R. Soc. Lond. B 1993 **340**, 393-404
doi: 10.1098/rstb.1993.0081

A method for routine monitoring of the aerial migration of insects by using a vertical-looking radar

A. D. SMITH[1], J. R. RILEY[1] AND R. D. GREGORY[2]

[1]*Natural Resources Institute Radar Unit, North Site, Leigh Sinton Road, Malvern, Worcestershire WR14 1LL, U.K.*
[2]*Department of Mathematics, University of Manchester, Oxford Road, Manchester M13 9PL, U.K.*

SUMMARY

Radar has been successfully used for over twenty years to study the flight behaviour of a variety of migrant insects. However, the complexity of the equipment and the time-consuming nature of data analysis procedures have precluded use of the technique for routine, long-term monitoring. We report here the development of a technique specifically intended to make such routine monitoring a practical proposition. The 3 cm radar transmits a vertical-looking beam which nutates about a vertical axis, and in which the plane of linear polarization is rotated. Overflying insects modulate the radar signal in a way which is related to their speed and direction of movement, their orientation, size, and shape. We have shown that all these parameters can be extracted from the complex Fourier transform of the returned radar signal, by using appropriate algorithms on a modern desk-top computer. The success of this development means that economic, automatic, and long-term monitoring of the density, direction of movement, orientation and composition of insect aerial faunas should now be possible.

1. INTRODUCTION

Radar has been used for nearly 25 years to study the aerial migration of a variety of insects (Schaefer 1976; Riley 1980, 1989; Reynolds 1988). These studies have greatly improved our understanding of nocturnal insect migration, and have emphasized its importance in the distribution and population dynamics of grasshoppers, locusts, moths and planthoppers (Schaefer 1976; Drake & Farrow 1983, 1985; Riley & Reynolds 1979, 1983, 1990; Riley *et al.* 1983, 1991; Reynolds & Riley 1988). However, the complexity of the equipment and the time-consuming nature of the data analysis procedures have hitherto precluded the use of radar for long term migration monitoring. We report here the development of a radar technique which should make it feasible to economically carry out routine, long-term observations of insect migratory flight. The technique substantially improves the capacity of radar to identify the species of insects detected by providing estimates of the mass of individuals and data related to their shape. It also yields individual displacement speed and direction, and body alignment azimuth. All the data can be automatically gathered and processed using a desk-top computer (for example, a top-of-the-range 486-based personal computer). The potential uses of the technique include monitoring the movement of insect pests of agriculture, and assessing long-term changes in the biomass and faunal diversity of insects caused by environmental perturbations.

2. THE EVOLUTION OF VERTICAL-LOOKING RADAR

(*a*) *Polarization rotation*

Over twenty years ago, Atlas *et al.* (1970*a*) reported the incidental detection of insect-like targets on their vertical-looking, meteorological radar and it was noted that the temporal variation of the signals from these targets provided a measure of their horizontal translation speed (Atlas *et al.* 1970*b*). We subsequently decided to exploit the potential of vertical-looking radar for entomological observations, and in 1975 deployed a vertical-looking system during our studies of locusts and grasshoppers in West Africa. This simple, pulsed radar operated with a wavelength (3.2 cm) more appropriate for insect detection than the 10 cm, continuous-wave, frequency-modulated system used by Atlas. The most significant difference, however, was that our radar transmitted a circularly symmetric, plane-polarized beam, in which the plane of polarization was continuously rotated (Riley & Reynolds 1979). The main reason for introducing polarization rotation was that we expected insects to scatter radar waves like prolate dielectric spheroids, so that echoes from long, thin insects would show more response to polarization rotation than short, fat ones. It was hoped that this difference could be used to supplement wing-beat frequency (often also available from the radar returns (Riley 1974; Schaefer 1976)) as a means of species identification. Rotating polariza-

Phil. Trans. R. Soc. Lond. B (1993) **340,** 393–404
Printed in Great Britain

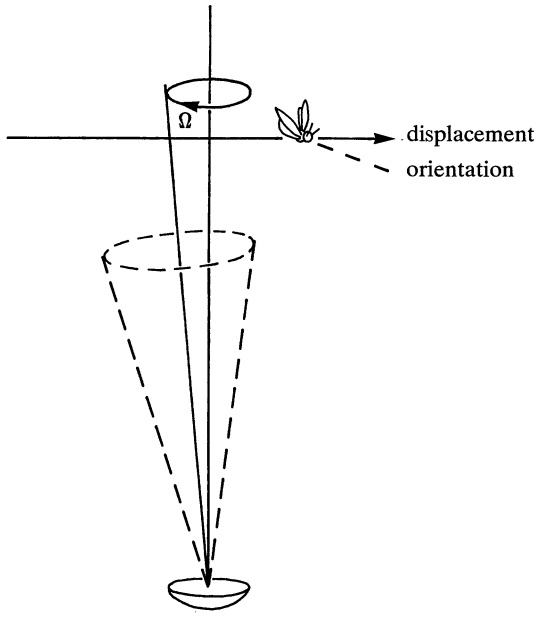

Figure 1. Elevation view of the VLR.

tion also promised to provide a means of accurately measuring the alignment of individual insects, because maxima in the signals scattered back to the radar were expected to occur when the electric vector in the radar waves became parallel with the insect major body axis.

(*b*) *Early experimental results*

In the event, the alignment measurement process proved to be very successful, and yielded novel measurements of insect heading distributions in both our own experiments (Riley & Reynolds 1979, 1986) and in concurrent and later airborne applications (Schaefer 1979; Hobbs & Wolf 1989; Wolf *et al.* 1990). We found, however, that extraction of body shape information was unfortunately frustrated by inadequate dynamic range in our receiver. It later became clear that there was a more fundamental problem with the body shape technique, because polarization dependence was found to be a function of body size as well as shape, at least in the case of larger insects (Riley 1985). In our experiments, target size could not be deduced from signal amplitude, because this is strongly influenced by the (unknown) distance of the insect targets from the radar beam centre.

(*c*) *Beam nutation*

Fortunately, information about the target-to-beam centre distance can be gained by causing the radar beam to rotate about an axis offset from the beam centre by a fraction of a beamwidth (figure 1). This nutation technique has been extensively developed for tracking radars (Dunn *et al.* 1970), and was exploited by Bent (1984) in an attempt to use radar to estimate the size of flying aphids. The aphid work was apparently frustrated by a lack of resources, and by the formidable problems of obtaining signals of adequate signal-to-noise ratio from such tiny targets. In the present work, we have applied the nutation principle to our rotating polarization radar, and have found that it allows us to measure the speed and displacement direction of individual overflying insects, their alignment direction, wingbeat frequency, and three parameters related to their size and shape. Measurements may be made simultaneously in many altitudinal ranges, and the data can be automatically processed by a desk-top computer.

3. THE PRINCIPLE OF OPERATION

(*a*) *Factors affecting the amplitude of the radar echoes*

The analysis which follows describes the signals returned by individual insects. The radar aerial consists of a vertically-pointing paraboloid reflector, fed by a double dipole feed (Silver 1949) which is offset slightly from the parabola axis of revolution. This assembly forms a transmit-receive beam which is approximately circularly symmetric, plane polarized in the plane containing the dipoles, and in which the gain falls off as a Gaussian function of the angular distance from the beam axis (Dunn *et al.* 1970). Rotation of the feed produces two effects: the plane of polarization rotates and the beam axis nutates about a vertical axis by a fraction of a beamwidth (figure 1). An insect which flies through the nutating beam is illuminated from below and will return time-varying radar echoes whose characteristics are determined by (i) the radar scattering properties of the insect, (ii) its trajectory.

If the insect is mirror symmetric in the vertical plane containing its body axis, then the cross-polarized radar back-scattering terms are zero and the mono-static back-scattering matrix of the insect may be written

$$\mathbf{S} = \begin{pmatrix} \sqrt{\sigma_{xx}} & 0 \\ 0 & e^{i\mu}\sqrt{\sigma_{yy}} \end{pmatrix} \tag{3.1}$$

where σ_{xx} is the maximum value of the (co-polarized) radar cross-section (RCS) as the plane of polarization† rotates, σ_{yy} is the RCS for the polarization direction orthogonal to that at which the maximum occurs, and μ is a phase angle (Kell & Ross 1970). For insects that are small compared with the radar wavelength, the (horizontal) axes *Oxy* are such that *Ox* is parallel to the insect's longitudinal body axis; for large insects however, the maximum RCS may occur when the plane of polarization is perpendicular to this body axis (Riley 1985; Aldous 1990). It follows (Aldous 1990) that, when the plane of polarization makes an angle ϕ with this *x*-axis, the RCS $\sigma(\phi)$ is given by

$$\sigma(\phi) = a_0 + a_2 \cos 2\phi + a_4 \cos 4\phi, \tag{3.2}$$

† We define the plane of polarization to be the plane containing the propagation direction and the **E**-vector.

PHILOSOPHICAL TRANSACTIONS OF THE ROYAL SOCIETY B BIOLOGICAL SCIENCES

where

$$a_0 = 3/8(\sigma_{xx} + \sigma_{yy}) + 1/4(\sigma_{xx}\sigma_{yy})^{\frac{1}{2}} \cos \mu,$$
$$a_2 = 1/2(\sigma_{xx} - \sigma_{yy}), \qquad (3.3)$$
$$a_4 = 1/8(\sigma_{xx} + \sigma_{yy}) - 1/4(\sigma_{xx}\sigma_{yy})^{\frac{1}{2}} \cos \mu.$$

The (real positive) constants a_0, a_2, a_4 (or equivalently σ_{xx},σ_{yy},μ) are determined by the size, shape and dielectric properties of the insect.

Because the insect is moving and the radar beam is nutating, the intensity of the beam incident upon the insect is not a constant. For our antenna the off-axis gain $G(r)$ is approximately Gaussian, that is

$$G(r) = G_0 \exp\left(-\frac{1}{2}kr^2\right), \qquad (3.4)$$

where G_0 is the on-axis gain, $k = 8 \ln 2$ and r is the (angular) distance from the instantaneous axis of the beam; this distance is measured in half-power beam-widths. On combining (3.2) and (3.4), the power of the signal received by the antenna at time t has the form

$$f(t) = C \exp(-kr^2)\{a_0 + a_2 \cos 2\phi + a_4 \cos 4\phi\}, \quad (3.5)$$

where C is a known constant containing the transmitted power and the target range; the time dependence is through r and ϕ.

Note: It is implicitly assumed in equation (3.5) that the scattering matrix remains unchanged during the target overflight. This requires the insect to maintain constant pitch and yaw, but the assumption is still not strictly valid for two reasons. Firstly, some modulation of RCS is to be expected as a consequence of wing beating, and secondly, the change of presented aspect which is caused by target translation relative to the radar, will also produce a change in RCS. Fortunately, wingbeat induced modulation is usually small (Riley 1973), and in any case will not affect the general form of $f(t)$. Aspect change is potentially more significant, at least in the case when insect dimensions are greater than the radar wavelength, because even the small (2°–3°) changes occurring during a beam transit may then produce quite large variations of RCS (Riley 1973). However, in the great majority of field recordings of individual insects which we have made with our 3 cm radar, the observed $f(t)$ (see example in figure 5*a*) corresponded very closely to simulated signals of the type shown in figure 5*b*. It thus seems reasonable to conclude that with radars of this and longer wavelengths, the scattering matrix of most insects may be taken to be effectively invariant during a transit of the radar beam, and that equation (3.5) provides an adequate description of $f(t)$.

(*b*) *Extraction of target parameters from f(t)*

The value of our vertical-looking radar (VLR) technique depends critically on the practicability of extracting, from measured values of $f(t)$, six parameters associated with each insect which overflies the radar. These are the speed V and displacement

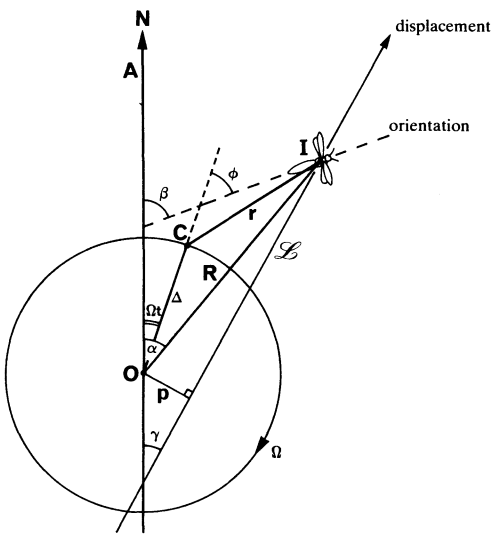

Figure 2. Plan of the geometry of the flight path and the VLR beam; the ***E***-vector is along OC.

direction γ, the body alignment β, and the three cross-section parameters a_0, a_2, a_4 which are related to the size and shape of the insect, and which (together with the wingbeat frequency) may provide important clues to its identity.

It is supposed that the insect I displaces along a horizontal straight line $\mathscr{L}$ with constant speed V. Figure 2 shows the horizontal plane containing $\mathscr{L}$. In this plane the VLR beam has centre C, which nutates about the fixed axis O with constant offset radius Δ and constant angular speed Ω; at time $t = 0$, OC lies along the fixed reference line OA. The line of flight $\mathscr{L}$ is specified by γ, the angle between $\mathscr{L}$ and OA, and p, the minimum distance of $\mathscr{L}$ from O; the insect is at this point of closest approach to O at some (unknown) time τ. Finally the body axis of the insect is supposed to make a constant angle β with OA, where $\beta \neq \gamma$ necessarily. The plane of polarization contains OC. Then the power received by the antenna is given by (3.5) with

$$\phi = \Omega t - \beta, \qquad (3.6)$$
$$r^2 = \Delta^2 + R^2 - 2\Delta R \cos(\Omega t - \alpha), \qquad (3.7)$$

where $\alpha = I\hat{O}A$ and $R(= OI)$ is given by

$$R^2 = V^2(t - \tau)^2 + p^2. \qquad (3.8)$$

On making these substitutions into (3.5) and after some trigonometry we obtain

$$f(t) = C\{a_0 + a_2 \cos 2(\Omega t - \beta) + a_4 \cos 4(\Omega t - \beta)\} \times e^{-k(\Delta^2 + p^2)} e^{-kV^2(t-\tau)^2} \exp 2k\Delta\{V(t - \tau) \cos(\Omega t - \gamma) + p \sin(\Omega t - \gamma)\}. \qquad (3.9)$$

In equation (3.9), $k = 8 \ln 2$ and C, Δ, Ω are known constants; the remaining constants a_0, a_2, a_4, γ, p, τ, V, β are properties of the insect and its flight.

If all the above constants are known, then it is a

PHILOSOPHICAL TRANSACTIONS OF THE ROYAL SOCIETY B BIOLOGICAL SCIENCES

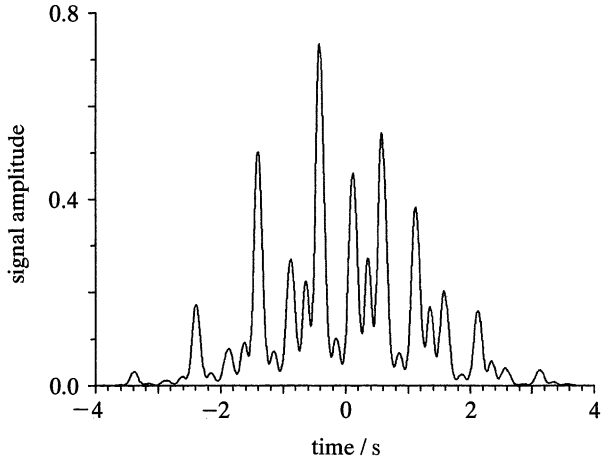

Figure 3. The simulated received signal amplitude for the data: $C=1$, $\Delta=0.1$, $\Omega=1$ Hz, $a_0=1.0$, $a_2=0.8$, $a_4=0.5$, $\gamma=65°$, $p=0.5$, $\tau=0.0$, $V=0.25$, $\beta=40°$.

simple matter to calculate the resulting signal amplitude; a typical simulated signal amplitude is shown in figure 3.

However, we need to solve the inverse problem to the above, namely: Given the signal amplitude function $f(t)$ and the constants C, Δ, Ω, how can we determine the 'insect constants' a_0, a_2, a_4, γ, V, β? (p, τ are not of interest although p must still be determined.) These parameters are extracted by considering the complex Fourier transform $F(\omega)$ of $f(t)$ defined by

$$F(\omega) = \int_{-\infty}^{\infty} f(t)\mathrm{e}^{i\omega t}\,\mathrm{d}t. \tag{3.10}$$

Because the general extraction procedure is quite involved, we will explain the method for the special case in which $a_2 = a_4 = 0$. (In this case β will also not appear in (3.9) and is therefore indeterminate.) The general case is treated in Appendix 2.

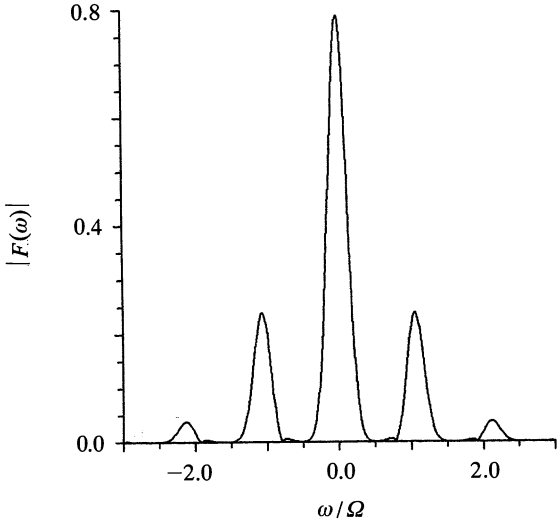

Figure 4. $|F(\omega)|$ against ω for the case in which $C=1$, $\Delta=0.1$, $\Omega=1$ Hz, $a_0=1.0$, $a_2=a_4=0$, $\gamma=65°$, $p=0.5$, $\tau=0.0$, $V=0.25$.

$F(\omega)$ has a much simpler form than $f(t)$. For the parameters used in figure 3 (but with $a_2 = a_4 = 0$) the absolute value of $F(\omega)$ is shown in figure 4. This was constructed directly from the signal $f(t)$ by numerical integration using the trapezium rule. The same can be done for real signals so that $F(\omega)$ can be found for any value of ω. We observe that $|F(\omega)|$ consists of a number of distinct peaks approximately centered on the points $\omega = n\Omega$ ($n = 0, \pm 1, \pm 2, \ldots$).

The transform $F(\omega)$ can also be found analytically in terms of the unknown parameters a_0, γ, V, p, τ. By using the generating formula (Watson 1944, pp. 14 and 77)

$$\exp\left[\frac{1}{2}z\left(w+\frac{1}{w}\right)\right] = \sum_{n=-\infty}^{\infty} w^n I_n(z), \tag{3.11}$$

the formula (3.9) for $f(t)$ can be written

$$f(t) = Ca_0\,\mathrm{e}^{-k(\Delta^2+p^2)}\,\mathrm{e}^{-kV^2(t-\tau)^2} \times \sum_{-\infty}^{\infty}\left(\frac{V(t-\tau)-ip}{\{V^2(t-\tau)^2+p^2\}^{\frac{1}{2}}}\right)^n \mathrm{e}^{in(\Omega t-\gamma)} I_n[2k\Delta\{V^2(t-\tau)^2+p^2\}^{\frac{1}{2}}]. \tag{3.12}$$

Here the functions $I_n(z)$ are the Bessel functions 'of imaginary argument' defined by $I_n(z) = (-i)^n J_n(iz)$. They are real positive and increasing functions when z is real positive and increasing. If we now substitute (3.12) into (3.10) and integrate term by term, we obtain

$$F(\omega) = C\frac{a_0}{V}\mathrm{e}^{-k(\Delta^2+p^2)} \sum_{n=-\infty}^{\infty} \mathrm{e}^{-in\gamma}\mathrm{e}^{i(n\Omega+\omega)\tau} R_n((\omega+n\Omega)/V), \tag{3.13}$$

where the functions $R_n(\alpha)$ are defined by

$$R_n(\alpha) = \int_{-\infty}^{\infty} \mathrm{e}^{-ks^2}\left(\frac{s-ip}{\{s^2+p^2\}^{\frac{1}{2}}}\right)^n I_n[2k\Delta\{s^2+p^2\}^{\frac{1}{2}}]\mathrm{e}^{i\alpha s}\mathrm{d}s, \tag{3.14}$$

the dependence on Δ, p being suppressed. ($s = V(t-\tau)$ is a new variable of integration.) The nth term of the series in (3.13) corresponds to the peak of $F(\omega)$ near $\omega = -n\Omega$ and if Ω/V is large enough§ ($\Omega/V > 12$ is sufficient) then these peaks will be effectively separated. We will assume that Ω is chosen large enough so that $\Omega/V > 12$ always holds. Then, in particular, the complex quantities $F(-n\Omega)$ are given by

$$F(-n\Omega) = C(a_0/V)\,\mathrm{e}^{-k(\Delta^2+p^2)}\mathrm{e}^{-in\gamma}R_n, \tag{3.15}$$

where R_n means the expression (3.14) with $\alpha = 0$ so that

$$R_0 = \int_{-\infty}^{\infty} \mathrm{e}^{-ks^2} I_0[2k\Delta\{s^2+p^2\}^{\frac{1}{2}}]\mathrm{d}s, \tag{3.16}$$

§ Here Ω is measured in radians per second and V in beamwidths per second.

Table 1. *Values of parameters extracted by the 'five peak' approximation, compared with their exact values, for various* Δ

	exact value	'five peak value' $\Delta = 0.1$, $\Omega = 1$ Hz	'five peak value' $\Delta = 0.2$, $\Omega = 1$ Hz	'five peak value' $\Delta = 0.3$, $\Omega = 1$ Hz
a_2/a_0	0.8	0.8000	0.8003	0.8004
a_4/a_0	0.5	0.5001	0.5010	0.5049
β	40°	40.00°	39.93°	39.68°
γ	65°	65.00°	64.99°	65.07°
p	0.5	0.5002	0.5007	0.5012
a_0/V	4.0	4.004	4.012	4.017
V	0.2500	0.2500	0.2498	0.2491

$$R_1 = -ip\int_{-\infty}^{\infty}\frac{e^{-ks^2}}{\{s^2+p^2\}^{\frac{1}{2}}}I_1[2k\Delta\{s^2+p^2\}^{\frac{1}{2}}]ds, \qquad (3.17)$$

$$R_2 = \int_{-\infty}^{\infty} e^{-ks^2}\left(\frac{s^2-p^2}{s^2+p^2}\right)I_2[2k\Delta\{s^2+p^2\}^{\frac{1}{2}}]ds. \qquad (3.18)$$

Note that the R_n depend only on the known beam offset Δ and the single parameter p. The values of $F(\omega)$ at the points $\omega = -n\Omega$ are of special importance and are denoted by F_n; these F_n may be calculated approximately from $f(t)$ by numerical integration of (3.10).

It follows from (3.15) that

$$F_0 = C(a_0/V)e^{-k(\Delta^2+p^2)}R_0, \qquad (3.19)$$

$$(F_1/F_0) = e^{-i\gamma}(R_1/R_0). \qquad (3.20)$$

Because R_0 is real and positive and R_1 is negative pure imaginary, it follows by taking the argument of (3.20) that γ is given by

$$\gamma = -\arg(F_1/F_0) - (\pi/2), \qquad (3.21)$$

while by taking the modulus of (3.20) it follows that p must satisfy the equation

$$p = \left|\frac{F_1}{F_0}\right|\frac{\int_{-\infty}^{\infty} e^{-ks^2}I_0[2k\Delta\{s^2+p^2\}^{\frac{1}{2}}]ds}{\int_{-\infty}^{\infty}\frac{e^{-ks^2}}{\{s^2+p^2\}^{\frac{1}{2}}}I_1[2k\Delta\{s^2+p^2\}^{\frac{1}{2}}]ds}. \qquad (3.22)$$

It is convenient to solve this equation for p numerically by iteration, taking as the starting value $p = |F_1/F_0|/(k\Delta)$, which is the solution in the limit as $\Delta \to 0$; when $\Delta = 0.1$, about two iterations were required to achieve three figure convergence (four when $\Delta = 0.2$).

Now that p is known, the ratio a_0/V is determined from (3.19) to be

$$a_0/V = e^{k(\Delta^2+p^2)}F_0/CR_0. \qquad (3.23)$$

The insect speed V can be determined from the 'width' of the central peak of $|F(\omega)|$. For ω near zero, we have from (3.13)

$$F(\omega) = C(a_0/V)e^{-k(\Delta^2+p^2)}e^{i\omega\tau}R_0(\omega/V) \qquad (3.24)$$

where $R_0(\alpha)$ is defined by (3.14); thus

$$|F(\omega)/F(0)| = |R_0(\omega/V)/R_0(0)|. \qquad (3.25)$$

Now choose some value ω' from the range $0 < \omega < \Omega/2$ such that‡ the left side of (3.25) lies between (say) 0.3 and 0.7. Then V must satisfy the equation

$$|R_0(\omega'/V)/R_0(0)| = |F(\omega')/F(0)|. \qquad (3.26)$$

This equation for V can be solved numerically by bisection, taking the initial range of ω'/V to be $2 \leqslant \omega'/V \leqslant 6$. Now that V is known, the remaining parameter a_0 can be found since the ratio a_0/V is already known from (3.23).

This completes the process of parameter extraction for the case in which $a_2 = a_4 = 0$. The general case is treated in Appendix 2 by the 'three peak' and 'five peak' approximations, which are extensions of the method described above. The 'five peak' approximation is a remarkably accurate method of parameter extraction. When applied to the signal shown in figure 3, the values obtained for the extracted parameters are given in the second column of table 1; the exact values are in the first column. The corresponding extracted values when $\Delta = 0.2, 0.3$ are given in columns 3 and 4.

(c) *The effect of signal noise*

The accuracy of the parameter extraction method in the presence of signal noise was investigated by generating pseudo-random signals with a normal amplitude distribution (Williams 1991), adding them to simulated values of $f(t)$, and then running the extraction routine on the resulting signal. Table 2 shows how the errors in the extracted parameters varied with the signal-to-noise ratio, when using simulation parameters appropriate for our field radar. The numerical extraction procedure is seen in this example to generate some (very small) errors even when no noise is added to the signal, but these errors would not be of significance in entomological applications, and can, in any case, be reduced by optimising the value of Δ. More importantly, the table shows that the extraction method is remarkably robust in the presence of noise, and that errors in the extracted quantities do not become excessive until the signal-to-noise ratio becomes less than 10 dB, and even at a value of 3.6 dB the errors in the trajectory data and the principal cross-section term would be acceptable in most cases. The reason for this robustness is that our

‡ This will put the point $\omega = \omega'$ near the steepest part of the central peak of $|F(\Omega)|$ and will give a more accurate value for V.

PHILOSOPHICAL TRANSACTIONS OF THE ROYAL SOCIETY B BIOLOGICAL SCIENCES

Table 2. *Examples of extracted parameters for various signal-to-noise ratios*

(Errors are shown in brackets. Signal-to-noise ratio is defined as $10 \times \log$ (signal maximum power/mean noise power). Target simulation parameters: $\beta = 34/214°$, $\gamma = 176°$, $V = 1.15$ beamwidth per second, $a_0 = 42 \times 10^{-4}$ cm^2, $a_2 = 33 \times 10^{-4}$ cm^2 and $a_4 = 2.6 \times 10^{-4}$ cm^2. Radar parameters: $\Delta = 0.25$ beamwidth, $\Omega = 6$ Hz, range gate sample rate = 300 Hz.)

signal: noise ratio/dB	insect alignment axis/deg	insect displacement direction/deg	insect displacement speed/beamwidth per second	radar cross-section terms/($10^{-4} \times$ cm^2)		
				a_0	a_2	a_4
∞	35/215 (+1°)	175 (−1°)	1.16 (+1%)	40 (−5%)	32 (−6%)	2.7 (+1%)
30	35/215 (+1°)	175 (−1°)	1.16 (+1%)	40 (−5%)	32 (−6%)	2.7 (+1%)
20	35/215 (+1°)	175 (−1°)	1.16 (+1%)	40 (−5%)	32 (−6%)	2.7 (+1%)
10	35/215 (+1°)	175 (−1°)	1.13 (−2%)	39 (−9%)	31 (−9%)	2.5 (−4%)
3.6	32/212 (−2°)	171 (−5°)	1.23 (+7%)	39 (−9%)	30 (−12%)	3.7 (+38%)

extraction method uses the values of the transform function $F(\Omega)$ at the points $\omega = 0, -\Omega, -2\Omega, \ldots, -5\Omega$, which are at (or close to) the peaks of $|F(\omega)|$; thus the errors induced by random noise are proportionally minimized.

4. EXPERIMENTAL RESULTS

We had an opportunity to test a prototype vertical-looking radar at the beginning of 1991 during a collaborative field study with CSIRO in Australia. The radar was operated for a fortnight, mostly during the late afternoon and evening, at Narrabri in New South Wales, while a conventional entomological scanning radar was in use nearby. Signals were obtained from 15 altitude ranges simultaneously, and were multiplexed and digitally recorded on a tape recorder. A technical description of the radar is given in Appendix 1.

(*a*) *Analysis of the recorded signals*

For some of the observational period, especially just after dusk, the signals from the radar range gates (especially the lower ones) became semi-continuous because insects were entering the volumes sampled by the radar in close succession. At other times however, returns from individual insects were well separated, and were seen to be very similar to the simulated example shown in figure 3, although of varying amplitude. These signals (an example is shown in figure 5*a*) were analysed using the five-peak method described above, and the six extracted parameters were then used to re-calculate $f(t)$ (see figure 5*b*) for comparison with the original signal. In almost all cases, the measured and re-constituted signals were found to be very similar, and this similarity gave us confidence that the assumptions made in the scattering model were valid. Some examples of the extracted parameters are listed in table 3. The table also gives estimates of the masses of the individual insects detected. The estimates were derived from the empirical formula for 3.2 cm wavelength:

$$m = (\sigma_{xx} \times 10^5/6.4)^{\frac{1}{2}} \qquad (4.1)$$

for $\sigma_{xx} < 10^{-1}$ cm^2 (Riley 1992). For higher values of σ_{xx}, where Mie or resonance effects occur, the relationship between mass and σ_{yy} found by Aldous (1990) is more appropriate:

$$\log m = 2.54 + 0.766 \log(\sigma_{yy}) + 0.179\{\log(\sigma_{yy})\}^2. \qquad (4.2)$$

In both expressions σ_{xx}, σ_{yy} are expressed in cm^2, and m in mg. All the targets had a mass less than 1000 mg, so the axis of x was taken to correspond to the alignment of the insect major body axis (Riley 1985, Aldous 1990).

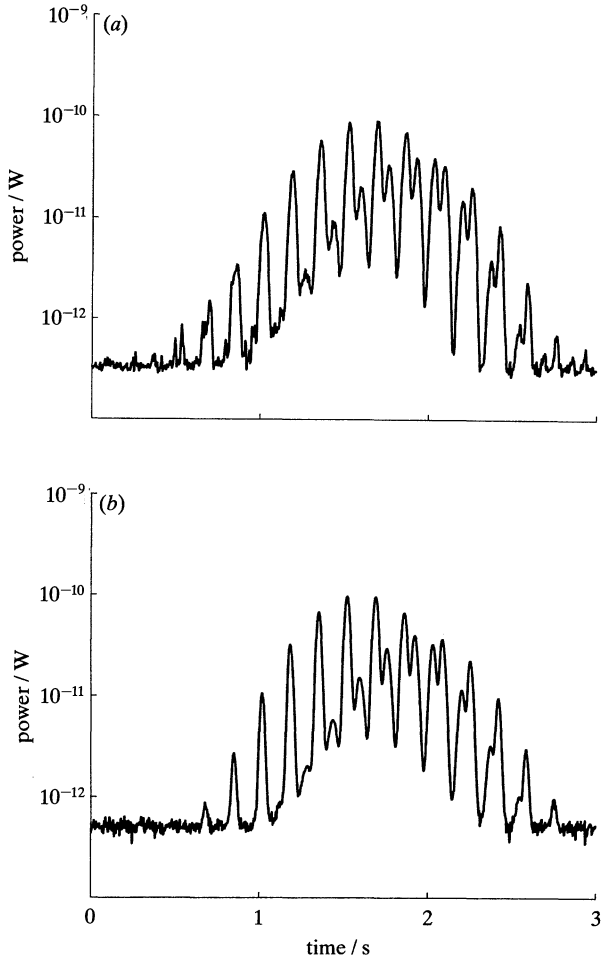

Figure 5. (*a*) Real signal, log (power). (*b*) Simulated signal, parameters as for experimental radar, log (power).

Table 3. *Examples of results extracted from data recorded at Narrabri, New South Wales, from 23 h 40 to 23 h 41 on 28 January 1991. The altitude range is 195 to 240 m*

scattering matrix terms			insect mass/mg	insect displacement speed/m s^{-1}	insect displacement direction/deg	insect alignment axis/deg
σ_{xx}/cm^2	σ_{yy}/cm^2	phase μ/deg				
3.2×10^{-1}	1.0×10^{-1}	70.3	89.7	10.8	313	37/217
1.4×10^{-2}	6.8×10^{-3}	77.0	14.8	7.5	9.6	134/314
1.6×10^{-2}	5.0×10^{-3}	78.9	15.8	7.7	10.8	133/313
1.1×10^{-1}	1.5×10^{-2}	90.1	54.7	9.9	52.6	151/331

(*b*) *Aerial density estimates*

A value for the insect aerial density was estimated by noting the fraction of time for which a range gate was occupied, and dividing the volume sensed within the gate by this fraction; this gave the volume occupied, on average, by one target. The sensed volume was calculated using the expression:

$$V_s = (c/2) \times \mathrm{d}t \times R^2 \times \pi \times (\theta/2)^2 \ \mathrm{m}^3, \qquad (4.3)$$

where c here is the velocity of light (3×10^8 m s^{-1}), $\mathrm{d}t$ = the range gate timing interval (selected to be in the range 0.1 to 1 μs), R is the distance of the gate from the radar (usually in the range 150–800 m), and θ is the beam nutation angle plus the angular width (both in radians) of the radar beam within which targets of a representative cross-section (chosen to be $\sigma_{xx} = 0.01$ cm^2) would return signals above the radar detection threshold. The average aerial density estimated in this way for the period during which the data in table 3 was acquired, was 0.3 insects per 10^4 m^3.

A more accurate assessment of density could be obtained if account were taken of the way in which target size distribution affects sensed volume (see Riley 1979), but this is not attempted here.

(*c*) *Wingbeat frequency modulation*

Standard Fourier analysis of the recorded signals showed few convincing examples of wingbeat frequency modulation in our recordings. The reason for this result is not clear, but we have found in the past that smaller insects appear to produce a lower amplitude of wingbeat modulation than larger grasshoppers and moths, and our size distribution data (figure 8) shows that in the experiments described here, the insects were rather small.

(*d*) *Comparison with measurements made by the scanning radar*

The VLR makes detailed measurements on many individual insects, whereas the scanning radar gives a more qualitative overview of the aerial population as a whole. Comparisons between the two systems are thus not exact, but nevertheless provide a check of the VLR results.

Figure 6 summarizes insect trajectory and body alignment data extracted from signals accumulated in five gates during the period 23 h 40 to 23 h 43 on 28 January 1991, over an altitude range of 195–540 m. The insects detected by the scanning radar during this period, and in the same altitude range, had average displacement speeds estimated to be 8–11 m s^{-1}, and were moving towards the north–northeast; both of these results are in excellent agreement with the data in figures 6*a*,*b*.

For part of the observational period, the scanning radar display showed evidence of the sectorial distribution of echoes characteristic of common orientation (Riley 1975), which indicated that there was a tendency for the detected insects to align their body axes in the 100°–280° direction. This result agrees less well with the alignment distribution shown in figure 6*c*, where the mean alignment axis was 131°–311°. However, the discrepancy probably arose because the sectorial pattern was discernible over only part of the altitude range, and was only weakly developed, so that determination of the common alignment axis was rather inexact. Very close agreement has previously been found between alignment axes deduced from sectorial patterning, and from distributions measured with (non-nutating) vertical-looking radar (Riley & Reynolds 1979).

A pilot balloon tracked by the scanning radar provided an estimate of the wind velocity at the range gate altitudes, at about 23 h 15. Vector subtraction of this data from the individual insect displacement velocities measured by the VLR produced the air speed and heading data shown in figure 7. Because the wind speed (9 m s^{-1}) was substantially higher than insect air speeds, these results are rather sensitive to errors in wind velocity measurements and to changes which may have occurred between the times of the balloon flight and the radar measurements. Nevertheless, the calculated heading distribution (figure 7*b*) is seen to be broadly consistent with the alignment distribution in figure 6*c*, and identifies its western half as the heading end. Most of the calculated air speeds (figure 7*a*) are within the range to be expected for smallish insects (2–4 m s^{-1}), and the mass distribution data shown in figure 8 suggests that the majority of the detected insects were, in fact, quite small (between 4 and 32 mg). There was no aerial netting data to provide an independent measure of insect mass distribution at altitude, but specimens trapped during the evening in a vehicle-mounted net were mostly small Lepidoptera, of length about 10 mm and estimated

PHILOSOPHICAL TRANSACTIONS OF THE ROYAL SOCIETY B BIOLOGICAL SCIENCES

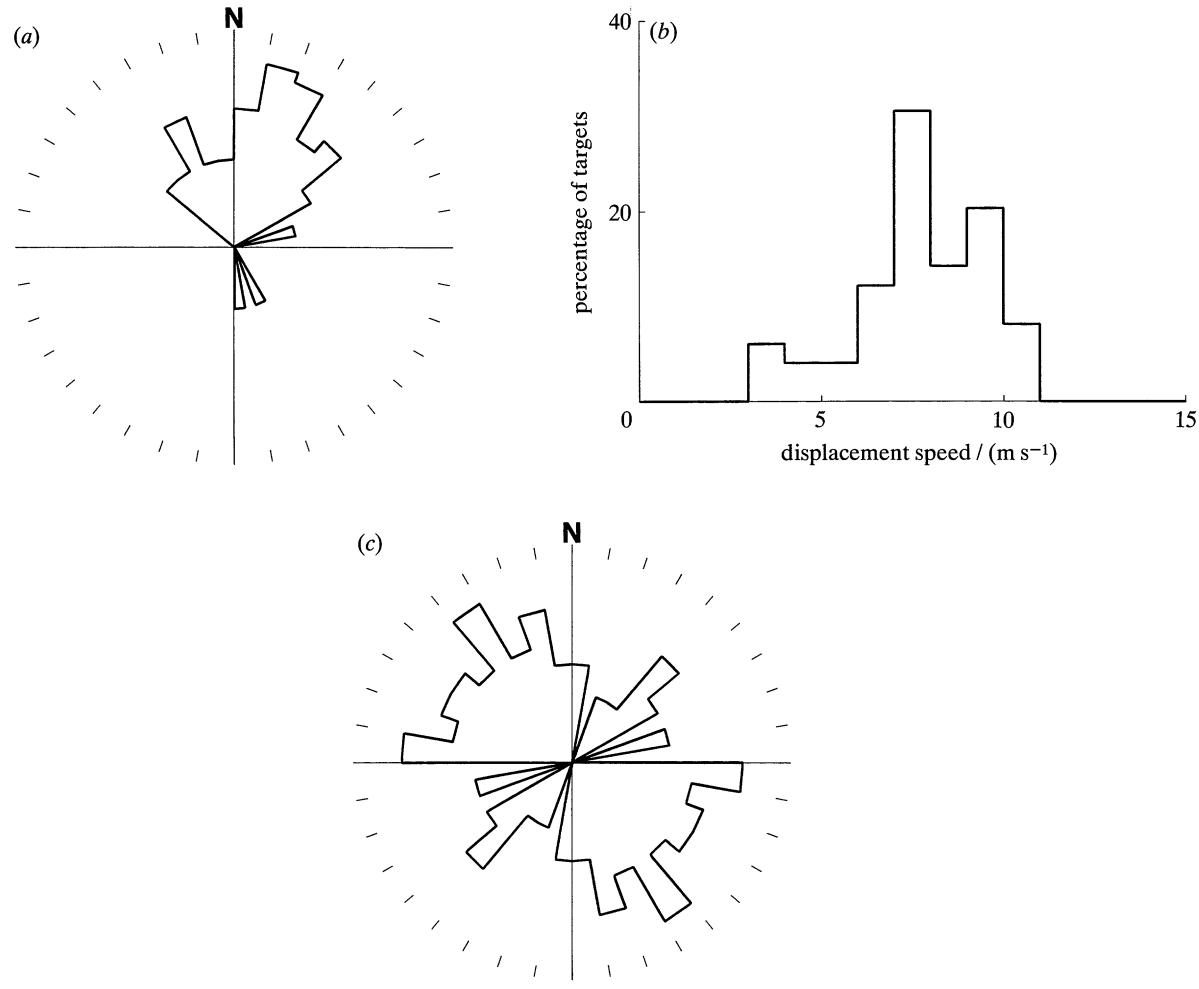

Figure 6. (*a*) Displacement polar histogram. (*b*) Displacement speed histogram. (*c*) Alignment polar histogram. Number of targets = 49.

mass 10–30 mg, so the radar results do not seem improbable. They are also consistent with the fact that the scanning radar was detecting, at its operational range of 900 m, insects presenting cross-sections greater than about 0.02 cm^2, i.e. with masses above 10–20 mg.

5. DISCUSSION

(*a*) *The validity of the model*

The similarity between examples of $f(t)$ measured by our 3.2 cm radar in the field, and those generated by simulations based on our overflying insect model, strongly suggest that the model provides an adequate description for $f(t)$, at least in the case of the insects observed in our Australian study. In addition, the general agreement between the flight trajectory data extracted from the vertical-looking radar with that observed on the scanning radar tends to validate convincingly both the model and the analysis procedure for $f(t)$.

(*b*) *Insect identification*

Further studies, supported by aerial sampling, are required to show how well the three cross-section terms, uniquely available from the vertical-looking radar, form useful insect identification features. However, it is already certain that the terms will, at the very least, greatly improve the capacity of radar to discriminate between species of different size. In the case of larger insects, wingbeat frequencies will usually be discernible in the radar returns, so a powerful, four-character identification scheme should be practicable.

(*c*) *Non-ideal signals*

The analysis method presented in this paper is appropriate only for situations where the aerial density of targets is such that less than one target at a time passes through the radar beam in each range gate interval. For our system, this corresponds to less than one insect per 12 000 m^3 at an altitude of 300 m. At higher densities, the shoulders of the Gaussian envelope of $f(t)$ become distorted in a way not described by our model, as echoes from sequential targets overlap. If overlapping targets are also in the same pulse volume, then interference between the reflected radar waves will also occur and may produce deep modulation of the combined signal (Blacksmith *et al.* 1965), as their differential range from the radar

PHILOSOPHICAL TRANSACTIONS OF THE ROYAL SOCIETY B BIOLOGICAL SCIENCES

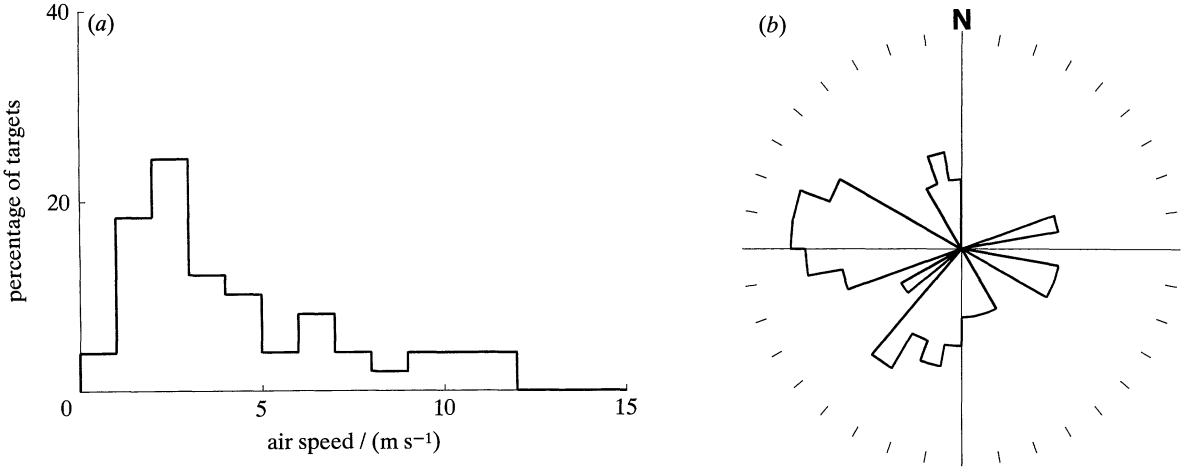

Figure 7. (*a*) Air speed histogram. (*b*) Heading polar histogram.

changes during the overflight. Distortion of the Gaussian envelope corrupts information about target size and translation speed, but the alignment angle and direction of displacement are encoded in the phase of the signals at frequencies Ω and 2Ω and can be recovered from selected segments of $f(t)$.

The problem of multiple targets can be avoided by using a very narrow radar beam and short range gates so that overlapping signals rarely occur. The disadvantage of this solution is that at times of low density overflight, the rate of target interception might be unacceptably low. In most cases, it will be desirable to have the capacity to vary the range gates and perhaps also the radar beamwidth, so that both high and low density overflights can be adequately monitored.

The more sensitive dependence of cross-section on aspect, to be expected in large insect species, may also produce signals not adequately described by our model, and more field studies with 3 cm radar are required to determine if this is the case.

(*d*) *Future developments and applications*

The full potential of the method described in this paper will become clear only when its species identification capability has been thoroughly demonstrated in a series of field studies in different environments. It also remains to determine whether a wavelength longer than 3 cm will be required to reduce the aspect sensitivity of cross-section which is a feature of the larger insects at 3 cm wavelength.

Nevertheless, it seems certain on present evidence that vertical-looking radar will provide a very powerful means to automatically observe insect flight at altitude, and will be especially useful in long-term studies of orientation behaviour and of migration. Because the system is based on the mature technology of marine radars and personal computers, it will be inexpensive, and can be expected to perform reliably over long periods. It is therefore uniquely suited to monitoring aerial pest movement for agricultural forecast and control schemes, perhaps deployed in networks or chains. Vertical-looking radar also holds considerable promise as a means of automatically and cheaply monitoring changes in the biodiversity of airborne insects.

We are grateful to Dr G. A. Bent for alerting us to the potential of the nutation technique, and to the Division of Entomology of CSIRO, Australia, for supporting the field trials of the vertical-looking radar. Thanks are also due to Dr. V. A. Drake and Mr. W. Rochester for their hospitality and collaboration, and for supplying data acquired by the scanning radar.

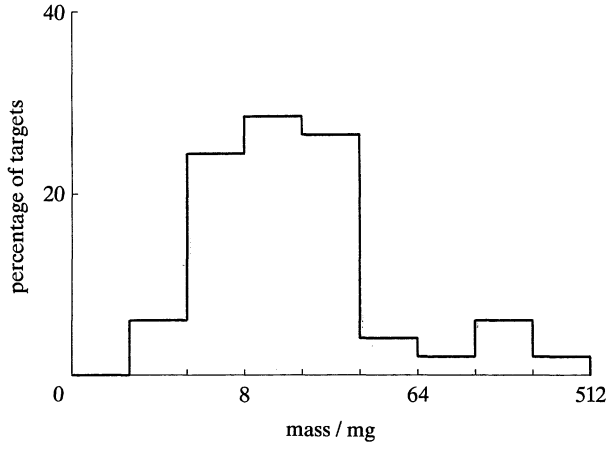

Figure 8. Mass distribution histogram.

APPENDIX 1. TECHNICAL DESCRIPTION OF THE RADAR

Our equipment is based on a simple marine radar transceiver which combines the virtues of being relatively inexpensive and rugged enough for field use. The transceiver was fitted with a precision log amplifier to increase the receiver's accuracy and dynamic range, and connected to a vertical-looking, parabolic antenna. The technical details of the radar are summarized in table A1. Signals from selected altitude ranges are captured by the use of 15 'range gates' which sample and hold echoes returning at set

Table A1. *VLR specification*

transmitter	
frequency	9.4 GHz
p.r.f.	1.5 kHz
pulse length	100 nS
receiver	
precision Logarithmic with low noise front end	
IF frequency	60 MHz
noise figure (including duplexer)	7 dB
IF bandwidth	20 MHz
antenna	
parabolic reflector with offset dipole feed	1.2 or 1.5 m
dipole rotation rate	6.01 Hz
dipole offset (in beamwidths)	0.1 to 0.5
data acquisition system	
primary sample rate (radar p.r.f.)	1.5 kHz
range gate channels	15
north marker channel	1
secondary sampling anti-alias filter cut off	100 Hz
secondary sample rate (12 bit A to D converter)	300.48 Hz
secondary samples per dipole revolution	50 per revolution per channel
data rate	4808 samples per second
multiplexer bit rate	62500 bits per second
housekeeping data rate	600 baud

intervals after the transmission of an outgoing pulse. Sampling takes place at the radar pulse repetition frequency, but the gate outputs are low-pass filtered and sampled at a lower frequency (300 Hz) which reduces by a factor of five the rate at which data must be processed or recorded. The signals from the gates are then multiplexed into one channel, with 'housekeeping' data on another.

APPENDIX 2. PARAMETER EXTRACTION IN THE GENERAL CASE

As in the special case treated in § 3, the parameters are extracted by considering the Fourier transform $F(\omega)$ of the signal $f(t)$. First consider the contribution of a_2 by setting $a_0 = a_4 = 0$. Then $f(t)$ is the same as in (3.12) except that a_0 is replaced by $a_2 \cos 2(\Omega t - \beta)$, which can be written

$$\tfrac{1}{2} a_2 e^{-2i\beta}) e^{2i\Omega t} + (\tfrac{1}{2} a_2 e^{2i\beta}) e^{-2i\Omega t}. \quad (A.1)$$

The Fourier transform of $f(t)$ will now be the superposition of two transforms, each like that shown in figure 4. The first has 'amplitude' $\frac{1}{2}a_2 e^{-2i\beta}$ instead of a_0 and is shifted to the left by 2Ω; the second has amplitude $\frac{1}{2}a_2 e^{2i\beta}$ and is shifted to the right by 2Ω.

The contribution of a_4 is similarly accounted for, and gives rise to two more transforms of amplitudes $\frac{1}{2}a_4 e^{\pm 4i\beta}$ shifted now by $\pm 4\Omega$. The general case then has a transform function $F(\omega)$ which is the superposition of five transforms, each of which is like that shown in figure 4. A typical example of the general behaviour of $|F(\omega)|$ is shown in figure A1.

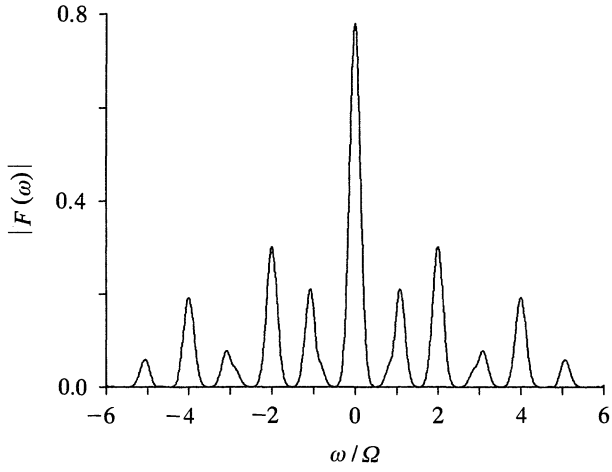

Figure A1. $|F(\omega)|$ against ω in the general case.

As a first approximation we shall assume that each of the five transforms which make up $F(\omega)$ consists of three peaks only‖; in figure 4 this means disregarding all peaks except those near $\omega = 0, \pm\Omega$. Subject to this 'three peak' approximation, there is only one contribution to each F_n for $n = 0, 2, 4, 5$ and two contributions for $n = 1, 3$, as follows:

$$F_0 = C(a_0/V) e^{-k(\Delta^2+\rho^2)} R_0, \quad (A.2)$$

$$F_1/F_0 = (e^{-i\gamma}(R_1/R_0)) + (a_2 e^{-2i\beta}/2a_0)\,(e^{-i\gamma}(R_1/R_0))^*, \quad (A.3)$$

$$F_2/F_0 = a_2 e^{-2i\beta}/2a_0, \quad (A.4)$$

$$F_3/F_0 = (a_2 e^{-2i\beta}/2a_0)\,(e^{-i\gamma}(R_1/R_0)) + (a_4 e^{-4i\beta}/2a_0)\,(e^{-i\gamma}(R_1/R_0))^*, \quad (A.5)$$

$$F_4/F_0 = a_4 e^{-4i\beta}/2a_0, \quad (A.6)$$

$$F_5/F_0 = (a_4 e^{-4i\beta}/2a_0)\,(e^{-i\gamma}(R_1/R_0))^*. \quad (A.7)$$

We can now begin the process of parameter extraction. Because a_0, a_2, a_4 are positive, it follows from (A.4) that

$$a_2/a_0 = 2|F_2/F_0| \quad (A.8)$$

and that

$$\beta = -\tfrac{1}{2} \arg (F_2/F_0). \quad (A.9)$$

Similarly from (A.6)

$$a_4/a_0 = 2|F_4/F_0|. \quad (A.10)$$

Equations (A.3), (A.5), (A.7) may be combined to give

$$G \equiv (F_1/F_0) - e^{-4i\beta}(F_3/F_0)^* + e^{4i\beta}(F_5/F_0) = e^{-i\gamma}(R_1/R_0). \quad (A.11)$$

As β is now known from (A.9), the left side G of

‖ This approximation becomes more accurate as $\Delta \to 0$. However, for very small Δ, the peaks near $\omega = \pm\Omega$ also become very small and this is undesirable since the information they contain will be lost.

PHILOSOPHICAL TRANSACTIONS OF THE ROYAL SOCIETY B BIOLOGICAL SCIENCES

Table A2. *Values of parameters extracted by the 'three peak' approximation, compared with their exact values, for various* Δ

	exact value	'three peak' value with $\Delta = 0.1$, $\Omega = 1$ Hz	'three peak' value with $\Delta = 0.2$, $\Omega = 1$ Hz
a_2/a_0	0.8	0.773	0.715
a_4/a_0	0.5	0.494	0.484
β	40°	39.0°	36.4°
γ	65°	66.0°	69.4°
p	0.5	0.495	0.471
a_0/V	4.0	3.85	3.39

(A.11) is also known, and this equation can be used to find γ and p as in § 3. The 'three peak' approximate determination of V is identical to that described in § 3.

When applied for instance to the signal shown in figure 3, the values obtained for the extracted parameters are those in the second column of table A2; the exact values are in the first column. The corresponding extracted values with $\Delta = 0.2$ are in column three. Clearly the accuracy of the 'three peak' approximation deteriorates with increasing Δ, and this restricts its use to small values of Δ. This restriction can be overcome by using an improved 'five peak' approximation for the basic transform. The 'five peak' approximation retains the F_0, $F_{\pm 1}$, $F_{\pm 2}$ of each basic transform and neglects F_n for $|n| \geqslant 3$; each basic transform is thus regarded as consisting of five peaks only. In this approximation we may write

$$\left.\begin{aligned} F_0 &= \hat{F}_0 + c\hat{F}_2^* + c^*\hat{F}_2, \\ F_2 &= \hat{F}_2 + c\hat{F}_0 + c^*\hat{F}_4, \\ F_4 &= \hat{F}_4 + c\hat{F}_2, \end{aligned}\right\} \tag{A.12}$$

and

$$\hat{G} \equiv (F_1/\hat{F}_0) - \mathrm{e}^{-4i\beta}(F_3/\hat{F}_0)^* + \mathrm{e}^{4i\beta}(F_5/\hat{F}_0) = \mathrm{e}^{-i\gamma}(R_1/R_0). \tag{A.13}$$

In (A.12), (A.13),

$$c = \mathrm{e}^{-2i\gamma}R_2/R_0 \tag{A.14}$$

and $\hat{F}_0$, $\hat{F}_2$, $\hat{F}_4$ are the contributions to F_0, F_2, F_4 from the 'three peak' theory; the terms involving c can be regarded as correction terms. Equations (A.12) and their complex conjugates can be arranged as a 5×5 set of linear equations to determine the $\hat{F}_n$ from the F_n, as follows:

$$\begin{pmatrix} 1 & c^* & 0 & c & 0 \\ c & 1 & c^* & 0 & 0 \\ 0 & c & 1 & 0 & 0 \\ c^* & 0 & 0 & 1 & c \\ 0 & 0 & 0 & c^* & 1 \end{pmatrix} \begin{pmatrix} \hat{F}_0 \\ \hat{F}_2 \\ \hat{F}_4 \\ \hat{F}_2^* \\ \hat{F}_4^* \end{pmatrix} = \begin{pmatrix} F_0 \\ F_2 \\ F_4 \\ F_2^* \\ F_4^* \end{pmatrix}. \tag{A.15}$$

In (A.15), the right side is known, but the matrix elements are functions of γ, p and are not yet known. A direct solution does not seem to be possible, but we may proceed iteratively as follows:

First use the 'three peak' method to determine values for γ, p. Now put these values into the matrix in (A.15) and solve for the $\hat{F}_n$; we can then find β (see (A.9)) by

$$\beta = -\tfrac{1}{2}\arg(\hat{F}_2/\hat{F}_0). \tag{A.16}$$

Substitute this value for β, and $\hat{F}_0$ from (A.15), into (A.13) and determine γ, p from this equation as described in the 'three peaks' theory with G replaced by $\hat{G}$. This determines more accurate values for γ, p and the iteration can begin again. When the values of γ, p have converged sufficiently we may finally use

$$a_2/a_0 = 2|\hat{F}_2/\hat{F}_0|, \tag{A.17}$$

$$a_4/a_0 = 2|\hat{F}_4/\hat{F}_0|, \tag{A.18}$$

$$a_0/V = \mathrm{e}^{k(\Delta^2 + p^2)}\hat{F}_0/CR_0. \tag{A.19}$$

The convergence of this iteration process is quite rapid; when $\Delta = 0.1$ the parameters are within 0.1% of their final values after about 2 iterations (4 when $\Delta = 0.2$, 6 when $\Delta = 0.3$).

In the 'five peak' theory the equation for V corresponding to (3.26) is

$$R_0(0)|F(\omega')| = |R_0(\omega'/V)\hat{F}_0 + \mathrm{e}^{-2i\gamma}R_2(\omega'/V)\hat{F}_2^* + \mathrm{e}^{2i\gamma}(R_2(-\omega'/V))^*\hat{F}_2|, \tag{A.20}$$

which can also be solved for V by bisection; all the other parameters which appear, that is γ, p, $\hat{F}_0$, $\hat{F}_2$, have already been determined.

Further 'multi-peak' approximations are possible, but would seem to be unnecessary in view of accuracy of the 'five peak' theory (see for instance the example of parameter extraction from a simulated signal by the 'five peaks' theory given in § 3, table 1). It is fair to regard the 'five peak' procedure as the solution of the problem of parameter extraction, at least for exact data.

REFERENCES

Aldous, A.C. 1990 Insect radar scattering cross-sections, Ph.D. thesis, Cranfield Institute of Technology.

Atlas, D., Metcalf, J.I., Richter, J.H. & Gossard, E.E. 1970*a* The birth of "CAT" and microscale turbulence. *J. atmos. Sci.* **27**, 903–913.

Atlas, D., Harris, F.I. & Richter, J.H. 1970*b* The measurement of point target speeds with incoherent non-tracking radar: insect speeds in atmospheric waves. *Proceedings of the 14th Radar Meteorology Conference, Tuscon, Arizona*, November 17–20, 1970, pp. 73–78. Boston: American Meteorological Society.

Bent, G.A. 1984 Developments in detection of airborne aphids with radar. *1984 British Crop Protection Conference—Pests and Diseases* pp. 665–674. Croydon: British Crop Protection Council.

Blacksmith, P., Hiatt, R.E. & Mack, R.B. 1965 Introduction to radar cross-section measurements. *Proc. IEEE* **58**, 901–920.

Drake, V.A. & Farrow, R.A. 1983 The nocturnal migration of the Australian plague locust *Chortoicetes terminifera* (Walker) (Orthoptera: Acrididae): quantitative radar observations of a series of northward flights. *Bull. ent. Res.* **73**, 567–585.

Drake, V.A. & Farrow, R.A. 1985 A radar and aerial-trapping study of an early spring migration of moths

(Lepidoptera) in inland New South Wales. *Aust. J. Ecol.* **10**, 223–235.

Dunn, J.H., Howard, D.D. & Pendleton, K.B. 1970 Tracking Radar. In *Radar handbook* (ed. M. I. Skolnik) pp. 21-1–21-54. New York: McGraw-Hill.

Hobbs, S.E. & Wolf, W.W. 1989 An airborne radar technique for studying insect migration. *Bull. ent. Res.* **79**, 693–704.

Kell, R.E. & Ross, R.A. 1970 Radar cross section of targets. In *Radar handbook* (ed. M. I. Skolnik) pp. 27-1–27-40. New York: McGraw-Hill.

Reynolds D.R. 1988 Twenty years of radar entomology. *Antenna* **12**, 44–49.

Reynolds, D.R. & Riley, J.R. 1988 A migration of grasshoppers, particularly *Diabolocatantops axillaris* (Thunberg) (Orthoptera: Acrididae) in the West African Sahel. *Bull. ent. Res.* **78**, 251–271.

Riley, J.R. 1973 Angular and temporal variations in the radar cross-sections of insects. *Proc. IEE* **120**, 1229–1232.

Riley, J.R. 1974 Radar observations of individual desert locusts (*Schistocerca gregaria* (Forsk.) (Orthoptera: Locustidae)). *Bull. ent. Res.* **64**, 19–32.

Riley, J.R. 1975 Collective orientation in night-flying insects. *Nature, Lond.* **253**, 113–114.

Riley, J.R. 1979 Quantitative analysis of radar returns from insects. In *Radar, insect population ecology and pest management* (ed. C. R. Vaughn, W. Wolf & W. Klassen) pp. 131–157. NASA Conf. Pub. 2070, Wallops Island, Virginia.

Riley, J.R. 1980 Radar as an aid to the study of insect flight. In *A handbook on biotelemetry and radio tracking* (ed. C. J. Amlaner & D. W. McDonald) pp. 131–140. Oxford: Pergamon.

Riley, J.R. 1985 Radar cross-section of insects. *Proc. IEEE* **73**, 228–232.

Riley, J.R. 1989 Remote sensing in entomology. *A. Rev. ent.* **34**, 247–71.

Riley, J.R. 1992 A millimetric radar to study the flight of small insects. *Electron. & Comms. Eng. J.* **4**, 43–48.

Riley, J.R. & Reynolds, D.R. 1979 Radar-based studies of the migratory flight of grasshoppers in the middle Niger area of Mali. *Proc. R. Soc. Lond.* B **204**, 67–82.

Riley, J.R. & Reynolds, D.R. 1983 A long-range migration of grasshoppers observed in the Sahelian zone of Mali by two radars. *J. Anim. Ecol.* **52**, 167–183.

Riley, J.R. & Reynolds, D.R. 1986 Orientation at night by high-flying insects. In *Insect flight: dispersal and migration* (ed. W. Danthanarayana) pp. 71–87. Berlin, Heidelberg: Springer-Verlag.

Riley, J.R. & Reynolds D.R. 1990 Nocturnal grasshopper migration in West Africa: transport and concentration by the wind, and the implications for air-to-air control. *Phil. Trans. R. Soc. Lond.* B **328**, 655–672.

Riley, J.R., Reynolds, D.R. & Farmery, M.J. 1983 Observations of the flight behaviour of the armyworm moth, *Spodoptera exempta*, at an emergence site using radar and infra-red optical techniques. *Ecol. ent.* **8**, 395–418.

Riley, J.R., Cheng, X.N., Zhang, X.X., Reynolds, D.R., Xu, G.M., Smith, A.D., Cheng, J.Y., Bao, A.D. & Zhai, B.P. 1991 The long distance migration of *Nilaparvata lugens* (Stål) (Delphacidae) in China: radar observations of mass return flight in the autumn. *Ecol. ent.* **16**, 471–489.

Schaefer, G.W. 1976 Radar observations of insect flight. *Symp. R. ent. Soc. Lond.* **7**, 157–197.

Schaefer, G.W. 1979 An airborne radar technique for the investigation and control of migrating pest insects. *Phil. Trans. R. Soc. Lond.* B **287**, 459–465.

Silver, S. 1949 *Microwave antenna theory and design.* (623 pages.) Maidenhead: McGraw-Hill, MIT Radiation Lab. Series.

Watson, G.N. 1944 *A treatise on the theory of Bessel functions.* (804 pages). Cambridge University Press.

Williams, M. 1991 Random sampling. *Beebug*, August/September issue, 24–28.

Wolf, W.W., Westbrook, J.K., Raulston, J., Pair, S.D. & Hobbs, S.E. 1990 Recent airborne radar observations of migrant pests in the United States. *Phil. Trans. R. Soc. Lond.* B **328**, 619–630.

Received 13 October 1992; accepted November 1992

PHILOSOPHICAL TRANSACTIONS OF THE ROYAL SOCIETY B BIOLOGICAL SCIENCES